



ELSEVIER

Contents lists available at ScienceDirect

Physica E

journal homepage: www.elsevier.com/locate/physye

Extraction and scattering analyses of 2D and bulk carriers in epitaxial graphene-on-SiC structure



S.B. Lisesivdin^{a,*}, G. Atmaca^a, E. Arslan^b, S. Çakmakyapan^b, Ö. Kazar^b, S. Bütün^{b,c},
J. Ul-Hassan^d, E. Janzén^d, E. Özbay^{b,e,f}

^a Department of Physics, Faculty of Science, Gazi University, Teknikokullar, 06500 Ankara, Turkey

^b Nanotechnology Research Center, Bilkent University, Bilkent, 06800 Ankara, Turkey

^c Department of Electrical Engineering and Computer Science, Northwestern University, 2145 Sheridan Road, Evanston, IL 60208, USA

^d Department of Physics, Chemistry and Biology, Linköping University of Technology, S-581 83 Linköping, Sweden

^e Department of Physics, Bilkent University, Bilkent, 06800 Ankara, Turkey

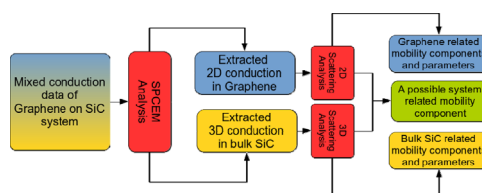
^f Department of Electrical and Electronics Engineering, Bilkent University, Bilkent, 06800 Ankara, Turkey

HIGHLIGHTS

- Mixed conduction in graphene on the SiC system is extracted.
- Scattering analyses of 2D carrier of graphene and 3D carrier of SiC were carried out.
- Mobility components and some phonon related parameters were calculated.
- A mobility component is suggested to be related to the graphene/SiC interaction.

GRAPHICAL ABSTRACT

The Simple Parallel Conduction Extraction Method (SPCEM) was used to extract mixed conduction in graphene on the SiC system. Extracted conduction channels related to graphene and bulk SiC layers were found. With the proper scattering analyses, mobility components of different mechanisms and some phonon related parameters were calculated. In addition to used scattering mechanisms, which are special to graphene or SiC layers, a temperature independent mobility component was observed in both scattering analyses with the same mobility limiting value. This mobility component is suggested to be related to the graphene/SiC interaction.



ARTICLE INFO

Article history:

Received 7 November 2013

Received in revised form

9 May 2014

Accepted 13 May 2014

Available online 21 May 2014

Keywords:

Graphene

2-dimensional

SiC

Hall effect

Scattering mechanism

ABSTRACT

Hall effect measurements of a graphene-on-SiC system were carried out as a function of temperature (1.8–200 K) at a static magnetic field (0.5 T). With the analysis of temperature dependent single-field Hall data with the Simple Parallel Conduction Extraction Method (SPCEM), bulk and two-dimensional (2D) carrier densities and mobilities were extracted successfully. Bulk carrier is attributed to SiC substrate and 2D carrier is attributed to the graphene layer. For each SPCEM extracted carrier data, relevant three-dimensional or 2D scattering analyses were performed. Each SPCEM extracted carrier data were explained with the related scattering analyses. A temperature independent mobility component, which may related to an interaction between graphene and SiC, was observed for both scattering analyses with the same mobility limiting value. With the SPCEM, effective ionized impurity concentration of SiC substrate, extracted 2D-mobility, and sheet carrier density of the graphene layer are calculated with using temperature dependent static magnetic field Hall data.

© 2014 Elsevier B.V. All rights reserved.

* Corresponding author. Tel.: +90 541 6602672; fax: +90 312 2122279.

E-mail address: bora@gazi.edu.tr (S.B. Lisesivdin).

1. Introduction

After Novoselov et al.'s inspirational study [1], graphene based systems and their unusual electrical properties attracted considerable attention [2–5]. Normally, a freestanding graphene, which has a band structure without a bandgap, can represent semiconductor behavior with the help of a substrate [6]. There are several growth methods including a substrate system such as mechanical cleavage, [1], epitaxial growth on SiC [7] or on transition metal substrates with chemical vapor deposition (CVD), [8] and chemical exfoliation of graphite [9] in order to form graphene structure, where the sublimation of SiC is one of the popular choices for large scale possible graphene growth.

Determining the mobility and carrier density of the carriers in a semiconductor system has great importance for a successful characterization of the structure. Charge carriers of the investigated system may include both 3-dimensional (3D) carriers and low-dimensional carriers which have different electrical transport properties. Therefore, extracting the electrical parameters of the carriers of a system can give important properties of the carriers and possible relations between them. After a successful growth of graphene on SiC substrate with the sublimation process, pure graphene conduction cannot be expected due to a possible bulk conduction of the SiC substrate itself [10]. An extraction of the 2-dimensional (2D) carrier of graphene and 3D bulk carrier of SiC substrate may give real values of the electrical parameters of the graphene layers formed on SiC substrate, and also the possible effect of the SiC substrate on graphene layers.

For the analysis of the Hall data with a parallel conduction problem, several methods are proposed or reported in the literature, such as the two-carrier model [11], multi-carrier fitting procedure (MCF) [12], mobility-spectrum analysis (MSA) [13], an MCF and MSA hybrid [14], the quantitative mobility spectrum analysis [15,16], and the maximum entropy mobility spectrum analysis [17]. All these methods have advantages and disadvantages for solving parallel conduction problem of different systems. Therefore, it is important to use the relevant method for a relevant problem. For structures such as a high electron mobility transistor or a modulation doped field effect transistor, which have a single bulk and a single 2D carrier type, the usage of the Simple Parallel Conduction Extraction Method (SPCEM) is proposed by Lisesivdin et al. [18].

In this study, experimental temperature dependent Hall mobilities and sheet carrier densities are used in SPCEM analysis. With the SPCEM, the temperature dependent mobilities and sheet carrier densities of 2D carrier of graphene and the bulk carrier of SiC substrate are calculated. With the successful scattering analyses for both carriers, some electrical transport related parameters are investigated.

2. Experimental

In this study, measurements were taken on epitaxial grown graphene layers on 4H-SiC (0 0 0 1), Si-face chemo-mechanically polished substrates. Graphene layers are grown on $10 \times 10 \text{ mm}^2$ sawed pieces that are taken from the central part of 4-in. substrate. The samples were exposed to a mixture of silane and hydrogen (0.006% silane in hydrogen) for 10 min at $1400 \text{ }^\circ\text{C}$. Graphene growth was performed at the same temperature under vacuum conditions ($\sim 5\text{--}9 \times 10^{-6}$ mbar) for 1 h. After graphene growth, the samples were cooled to $500 \text{ }^\circ\text{C}$ in vacuum. The growth cell was then filled with hydrogen to a pressure of 500 mbar and a one hour intercalation process was completed at $700 \text{ }^\circ\text{C}$. For the Hall measurements, by using the Hall bar geometry (Fig. 1, inset), a home-made photomask was fabricated with electron beam lithography in order to perform each fabrication step with optical lithography. Ti/Au (20 nm/100 nm) Ohmic contacts were deposited by an electron beam evaporator and then followed by the standard lift-off process. For the Hall measurements, $500 \text{ }\mu\text{m}$ by $1100 \text{ }\mu\text{m}$ Hall bars were fabricated. After Hall bar fabrication, Ti/Au (30 nm/220 nm) metal interconnect lithography was carried out.

The temperature dependent direct-current Hall effect measurements were taken from 1.8 to 200 K by using a Cryogen-free superconducting magnet system (Cryogenics Ltd., Model no. J2414) under a static magnetic field ($B=0.5 \text{ T}$). For measurements, a constant current source (Keithley 2400) and a nanovoltmeter (Keithley 2182A) were used. In measurements, current through the sample was intentionally kept low as $50 \text{ }\mu\text{A}$ to ensure ohmic conditions. Therefore, the 2D electrons were in thermal equilibrium with the graphene lattice even at low temperatures. One-two layer graphene formation is verified with standard Raman measurements which are taken with a Jobin Yvon Horiba Raman spectroscopy system. For Raman measurements, an excitation source, a He-Ne excitation laser with a 532 nm wavelength (2.33 eV) was used.

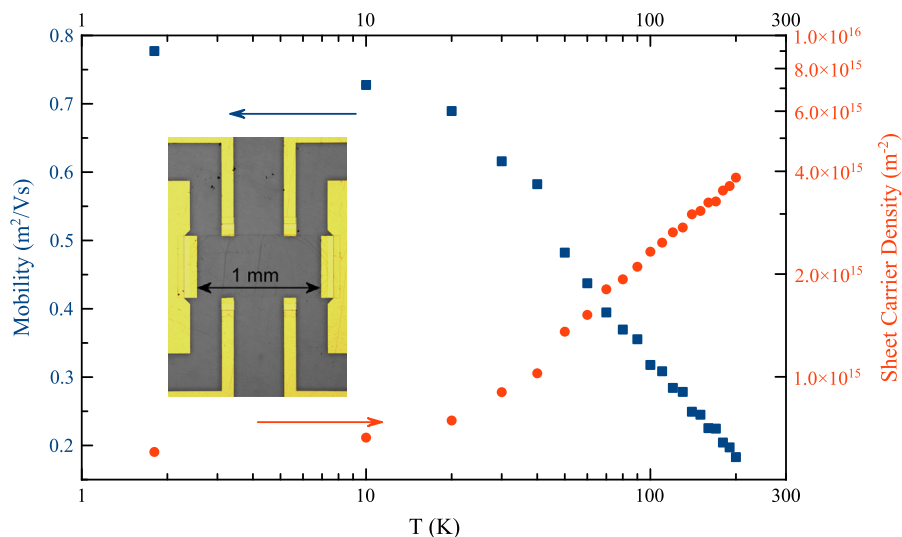


Fig.1. Temperature dependent electron mobility and sheet carrier density values. Inset: fabricated Hall bar structure.

3. Theory

3.1. SPCEM

The SPCEM has some assumptions, and these assumptions are the reason why it can be used for a structure with one bulk and one 2D carrier type:

- (1) 2D carrier and bulk carrier are two main carriers in the investigated structure.
- (2) Bulk carriers are presumed to be frozen at low temperatures. Therefore, at the lowest temperature, the experimental Hall carrier density can be accepted to be caused by only 2D carriers.
- (3) 2D carrier densities are accepted as temperature independent [19]. Therefore, temperature dependent change in measured carrier density is accepted to be caused by the thermal activation of bulk carriers only.
- (4) The 2D-carriers and bulk carriers' densities are approximately in the same order.

As mentioned above, the temperature independent carrier density is typical of 2D systems [19]. In a number of studies, 2D dominant Hall carrier densities slightly increase with increasing temperature due to the thermal activation of bulk carriers [20,21]. After implementing a successful parallel conduction extraction, 2D carrier densities showed temperature independent behavior [15,22,23]. Also, dominant 2D carrier density may show a decrement with increasing temperature in some semiconductor heterostructures including GaAs-based structures [24]. This is caused by the interaction between 2DEG electrons and bulk electrons with the trapping of DX-centers at the doped barrier at higher temperatures [25], which is not expected in a graphene-on-SiC system, and also not applicable with SPCEM. For graphene/SiC systems, Yu et al. suggested a drastically increase in carrier density with increasing temperature due to a band gap opening in the overlying graphene layer [10]. This gap opening phenomenon is sourced by the breaking of the sublattice symmetry by the buffer layer [10]. In their study, Yu et al. calculated the band gap of the related graphene layers and found values between 0.16 and 0.27 eV with the help of expression for carrier intrinsic excitation of conventional semiconductors

$$n_H = \sqrt{N_c N_v} e^{-E_g/2k_B T}, \quad (1)$$

where n_H , N_c , N_v , E_g , k_B and T are Hall carrier density, effective densities of states for conduction and valance bands, effective band gap, Boltzmann constant and lattice temperature, respectively.

For the mobilities of the bulk carrier μ_{Bulk} and the 2D carrier μ_{2D} , the following approximations can be found by the investigation of the magnetic field dependent conductivity tensors and their derivatives [18]:

$$\mu_{2D} \cong \mu_H \sqrt{\frac{n_H}{n_{2D}}}, \quad (2)$$

$$\mu_{Bulk} \cong \mu_H \frac{n_H - n_{2D}}{n_H} = \mu_H \frac{n_{Bulk}}{n_H}. \quad (3)$$

where μ_H is the experimental Hall mobility at a single magnetic field. All carrier density and mobility values presented in Eqs. (2) and (3) are the values that will be taken at a single magnetic field. In Lisesivdin et al.'s study, Eqs. (2) and (3) are proposed to be valid at low and high magnetic fields, respectively. Here, high magnetic fields value can be suggested as $B > 1/\mu$. For the structures with mobilities $\mu_H > 1 \text{ m}^2/\text{Vs}$, required magnetic field value will be low. Therefore, it is possible to use a single magnetic field. At the lowest temperature available, $n_{2D} = n_H$ is

taken and for all temperatures n_{2D} is accepted as temperature independent. For temperature dependent bulk carrier density, $n_{Bulk} = n_H - n_{2D}$ is used. Here, reader may think that for a two carrier system like our only total conductivity can be given as $\sigma_{Bulk} = \sigma_H - \sigma_{2D}$. And therefore, $n_{Bulk} = n_H - n_{2D}$ case can be seen true only for $\mu_H = \mu_{Bulk} = \mu_{2D}$. However, it is not true and both $\sigma_{Bulk} = \sigma_H - \sigma_{2D}$ and $n_{Bulk} = n_H - n_{2D}$ can be true for different bulk and 2D mobility value pairs. With the assumptions written above, the conductivities of the calculated carriers are known to have some error at the mid-temperatures of the investigated temperature interval [18]. However, at the lowest and highest investigated temperatures, the results of SPCEM become more satisfying [18]. At the lowest investigated temperatures, total mobility of the system (here, it is the experimental μ_H) is predominantly described by μ_{2D} because all bulk carriers are accepted to be frozen at those temperatures. At the highest investigated temperatures, total mobility of the system approaches a near factor of μ_{Bulk} because of the high number of activated bulk carriers. Therefore, it is easy to see that the lowest and the highest investigation temperatures directly determine the success of the technique.

3.2. Scattering mechanisms

The scattering mechanisms of bulk carriers and 2D-carriers are well known for many systems [26–28]. The analytical expressions of the bulk and 2D scattering mechanisms, which are used in this study, are summarized in the following subsections.

3.2.1. Scattering mechanisms used for bulk carriers

Three main scattering mechanisms that are involved because of phonon and impurity interactions are considered in this study. The parameters of SiC that are used in bulk scattering analysis are presented in Table 1 [29–33].

3.2.1.1. Ionized impurity scattering. Ionized impurity scattering is an elastic scattering process that happens at specific scattering centers. According to the Brooks–Herring model, the mobility limited by ionized impurity scattering mechanism is given as [34]

$$\mu_{II} = \sqrt{\frac{128(k_B T)^3}{m^* \pi^3} \frac{(4\pi \epsilon_s)^2}{Z^2 e^3 N_{IMP} [\ln [1 + \beta^2] - \beta^2 / (1 + \beta^2)]}}. \quad (4)$$

where m^* is the effective mass, Z is the charge of each ionized atom that is taken as unity, T is the lattice temperature, ϵ_s is the static dielectric constant, N_{IMP} is the density of ionized impurities in the crystal, and β is described as

$$\beta = \frac{2m^*}{\hbar} \lambda_D \sqrt{\frac{2}{m^*} 3k_B T}, \quad (5)$$

Table 1

Values of various parameters of SiC used in the bulk scattering calculations [29–33].

Parameter	Value
Effective mass (m^*)	0.29
ϵ_s	10.03
ϵ_0 ($\times 10^{-12}$ F/m)	8.85
$\hbar \omega_{PO}$ (meV)	197
E_D (eV)	18
c_{LA} ($\times 10^{11}$ N/m ²)	5.07

where λ_D is the 3D Debye screening length [28] and it is described as

$$\lambda_D = \sqrt{\frac{k_B T \epsilon_s}{e^2 n_{\text{Bulk}}}} \quad (6)$$

3.2.1.2. Polar optical phonon scattering. Polar optical phonon scattering is the dominant scattering mechanism at higher temperatures [35]. For the longitudinal polar optical phonon (LO-phonon) scattering, a simple mobility expression was used with a momentum relaxation time term

$$\mu_{\text{PO(Bulk)}} = \frac{e \tau_m}{m^*} e^{\hbar \omega_{\text{PO}} / k_B T}, \quad (7)$$

where $\hbar \omega_{\text{PO}}$ is the polar optical phonon energy and τ_m is the momentum relaxation time related to this scattering.

3.2.1.3. Acoustic phonon scattering. The scattering of electrons by acoustic phonons by both piezoelectric (PE) polarization fields and the deformation potential (DP) must be taken into account for the acoustic phonon scattering. The deformation potential scattering limited mobility is given by [27]

$$\mu_{\text{DP(Bulk)}} = \frac{\pi \hbar^3 c_{\text{LA}} e}{E_D^2 k_B T m^* k} \left[1 - \frac{q_{s3D}^2}{k^2} + \frac{q_{s3D}^4}{8k^4} \left(3 \ln \left[1 + \left(\frac{2k}{q_{s3D}} \right)^2 \right] - \frac{1}{1 + (q_{s3D}/2k)^2} \right) \right]^{-1}, \quad (8)$$

where E_D is the deformation potential constant, k is the electron wave vector and q_{s3D} is the reciprocal screening length in 3D

$$q_{s3D}^2 = -\frac{e^2}{\epsilon_s} \int \frac{df(E)}{dE} N(E) d(E), \quad (9)$$

where $f(E)$ is the Fermi–Dirac function and $N(E)$ is the density of states function. The limiting mobility for acoustic phonon scattering by a piezoelectric effect is given as [27]

$$\mu_{\text{PE(Bulk)}} = \frac{2\pi \epsilon_s \hbar^3 k}{K^2 e k_B T m^* 2} \left[1 - \frac{q_{s3D}^2}{k^2} + \frac{q_{s3D}^4}{8k^4} \left(3 \ln \left[1 + \left(\frac{2k}{q_{s3D}} \right)^2 \right] - \frac{1}{1 + (q_{s3D}/2k)^2} \right) \right]^{-1} \quad (10)$$

where K is the electromechanical coupling coefficient. With the help of Matthiessen's rule and Eqs. (8) and (10), the total acoustic phonon limited mobility ($\mu_{\text{AC(Bulk)}}$) can be calculated as

$$\frac{1}{\mu_{\text{AC(Bulk)}}} = \frac{1}{\mu_{\text{DP(Bulk)}}} + \frac{1}{\mu_{\text{PE(Bulk)}}}. \quad (11)$$

3.2.2. Scattering mechanisms used for 2D-carriers

In the investigation of total limited mobility in graphene on SiC systems (μ_{2D}) [32], longitudinal acoustic (LA) phonon scattering limited mobility (μ_{LA}) [36,37], remote interfacial phonon (RIP) scattering limited mobility (μ_{RIP}) [38], and a temperature independent scattering mobility term (μ_0) are used in Matthiessen's rule as [32]

$$\frac{1}{\mu_{2D}} = \frac{1}{\mu_{\text{LA}}} + \frac{1}{\mu_{\text{RIP}}} + \frac{1}{\mu_0}. \quad (12)$$

Table 2

Values of various parameters of graphene used in the 2D-scattering calculations [36,39,40].

Parameter	Value
D_A (eV)	18
ρ_s ($\times 10^{-7}$ kg/m ²)	7.6
v_s ($\times 10^4$ m/s)	2.1
v_s ($\times 10^6$ m/s)	1.0

The parameters of graphene that are used in 2D scattering analysis are presented in Table 2 [36,39,40].

3.2.2.1. LA phonon scattering. The limited mobility for dominant LA phonon scattering in graphene can be given as [36]

$$\mu_{\text{LA}} = \frac{4e \hbar \rho_s v_s^2 v_F^2}{n_{2D} \pi D_A^2 k_B T}, \quad (13)$$

where D_A , ρ_s , v_s , v_F and k_B are graphene related deformation potential, 2D mass density of graphene, LA phonon velocity, Fermi velocity of graphene and Boltzmann constant, respectively. The material parameters for Eq. 13 are presented in Table 2.

3.2.2.2. RIP phonon scattering. The RIP scattering in graphene is caused by optical phonons at the surface and subsurface of the graphene layer [38]

$$\mu_{\text{RIP}} = \frac{1}{n_{2D} e} \left[\sum_i \left(\frac{C_i}{\exp(E_i k_B T) - 1} \right) \right]^{-1}, \quad (14)$$

where C_i and E_i are fitting parameters for coupling strength and phonon energy, respectively.

3.2.2.3. Temperature independent scattering terms. The temperature independent scattering mobility term (μ_0) includes Coulomb scattering (μ_C) and short-range scattering (μ_{SR}) terms as

$$\frac{1}{\mu_0} = \frac{1}{\mu_C} + \frac{1}{\mu_{\text{SR}}}. \quad (15)$$

Short range scattering is known to inversely dependent to carrier density [10] as $\mu_{\text{SR}} = A/n_{2D}$, where A is a constant. In this study, 2D carrier density is temperature independent because of the 2nd assumption of SPCEM. Therefore, short range scattering is constant for all studied temperature range. Because μ_C is also constant, it is impossible to calculate the contribution of each scattering term to μ_0 . Therefore, instead of μ_C and μ_{SR} , μ_0 is calculated in our calculations.

4. Results and discussion

Fig. 1 shows the temperature dependence of Hall mobilities (μ_H) and Hall sheet carrier densities (n_H) of the investigated samples at static magnetic field density of 0.5 T and the temperature range of $T = 1.8$ –200 K. The temperature dependence of Hall mobility starts decreasing above 10 K. Sheet carrier density also becomes nearly temperature independent below 10 K. With the increasing temperature, sheet carrier density tends to increase rapidly to a value of $4 \times 10^{15} \text{ m}^{-2}$ at 200 K, which is nearly four times higher than the value at 1.8 K. These thermally induced carriers mostly originate from the SiC bulk layer that is laid under the graphene layer. At 1.8 K, electron mobility is calculated as high as $0.78 \text{ m}^2/\text{V s}$.

Because of the existing thermally induced bulk carriers, SPCEM analysis is carried out with the use of the temperature dependent Hall data to separate the 2D and bulk carriers at each temperature step. SPCEM analysis is carried out at a single low magnetic field (0.5 T) to eliminate the possible effects of oscillations in resistivity at low temperatures and high magnetic fields. The SPCEM results are shown in Fig. 2. The mobilities of both 2D and bulk carriers, which are shown in Fig. 2(a), are found to be influenced by the polar optical phonon scattering at high temperatures [41]. The bulk mobility decreases with decreasing temperature as expected because of the ionized impurity scattering at low temperatures [42]. In Fig. 2(b), the sheet carrier densities of both 2D and bulk

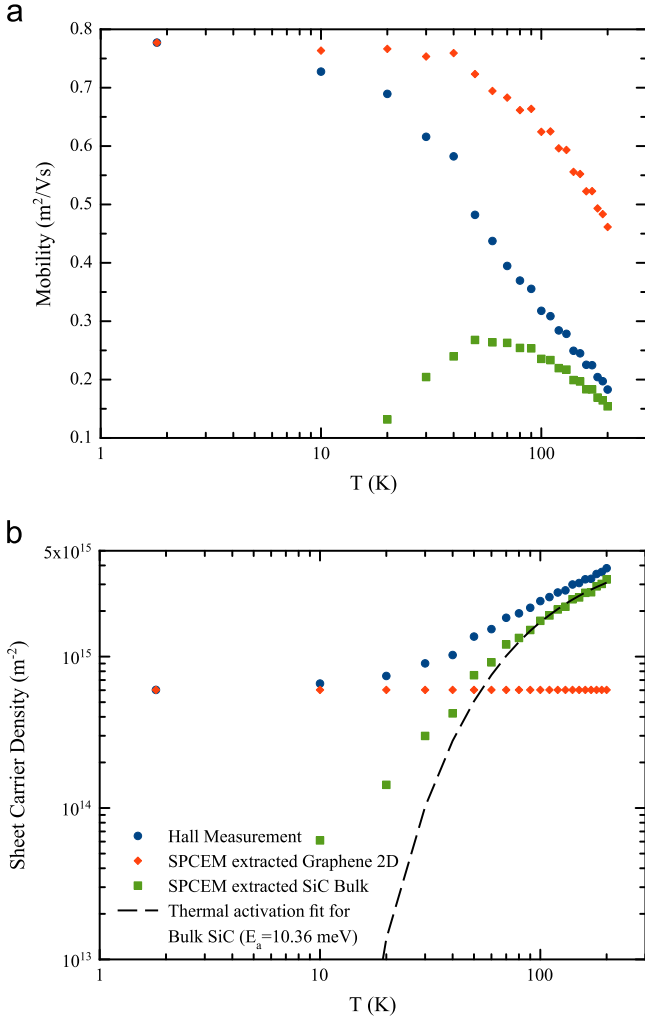


Fig. 2. (a) Mobilities and (b) sheet carrier densities of Hall measurement and SPCEM extracted 2D (graphene) and bulk (SiC) carriers. Thermal activation fit for bulk SiC is shown with dashes.

carriers are shown. The density of the 2D-carrier is accepted as temperature independent as stated before and the bulk carrier density decreases with decreasing temperature due to carrier freeze-out. In this study, Fermi level's position is assumed to be fixed with the changing temperature for a graphene/SiC system. Therefore, the extracted 2D-carrier and bulk carriers are to be related to the graphene layer and SiC substrate, respectively.

For a possible thermally activated donor level in bulk SiC, a fit with an activation energy (E_a) of 10.36 meV is also shown in Fig. 2(b). However, this number is smaller than the free-exciton value, and most of the known donor levels for the known impurities of 4H-SiC [10,43–45]. Since this value is smaller than Yu et al.'s 0.16–0.27 eV of band gap opening case, we do not believe that there is a possibility of band gap opening in our study [10]. Even with low values, a thermally activated state in bulk SiC case, which is also suitable for SPCEM, is more possible than a band opening case [10,46].

In Fig. 3, the scattering analysis of an SPCEM extracted 2D-carrier is shown by using the analytical expressions that are given in Section 3.2.2. For the RIP scattering, E_i and C_i are used as fitting parameters for 2 phonon modes. E_1 corresponds with a surface phonon mode of 4H-SiC and its value is 116 meV [47]. C_2 and E_2 correspond with another phonon mode [32]. We obtained the fitting parameter E_2 as 6.37 meV. For LA-phonon scattering, the mobility limiting values start from 521 $\text{m}^2/\text{V s}$, which is practically

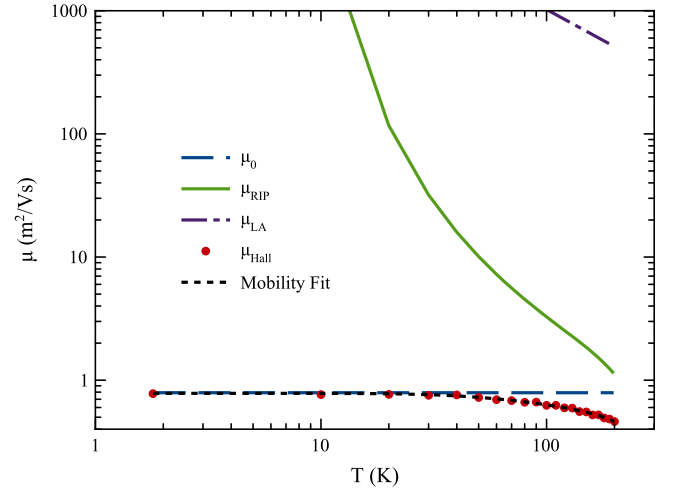


Fig. 3. Scattering analysis of SPCEM extracted 2D-carrier.

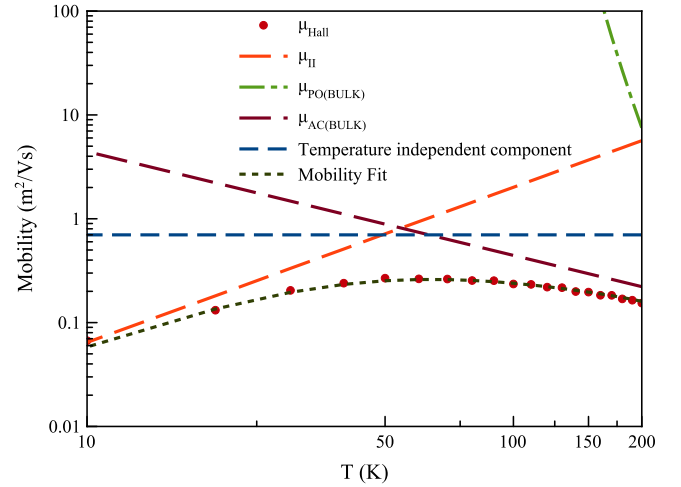


Fig. 4. Scattering analysis of SPCEM extracted bulk carrier.

ineffective on total mobility. In addition to RIP and LA-phonon, the temperature independent mobility limiting term μ_0 is found as 0.73 $\text{m}^2/\text{V s}$.

In order to calculate the density of the ionized impurities that influences the bulk mobility at lower temperatures, scattering analysis on temperature dependent bulk mobilities was implemented. A successful bulk scattering analysis based on the scattering mechanisms listed in Section 3.2.1 is shown in Fig. 4. Because of the maximum temperature 200 K, intervalley scattering is not included in the calculation [48]. In addition, optical phonon scattering is not effective in the studied range. The total mobility is then fitted using Matthiessen's rule. Ionized impurity scattering is the dominant scattering mechanism up to 50 K. Mobility limiting of ionized impurity scattering is calculated with the SPCEM extracted bulk carrier density, which is used in Eq. 4 and gives a successful fit at low temperatures. Above 50 K, mobility is mostly limited by acoustic phonon scattering. An important temperature independent scattering component with a magnitude of 0.73 $\text{m}^2/\text{V s}$ is seen in the whole studied temperature range. From the bulk scattering analysis, ionized impurity concentration and the momentum relaxation time for LO-phonons are determined as $1.5 \times 10^{20} \text{ m}^{-3}$ and $2.0 \times 10^{-12} \text{ s}$, respectively. The deformation potential constant is used as 18 eV, which is the value found from 2D-analysis. The agreement between the fitted and measured results is excellent. The obtained results for ionized

impurity concentration and the momentum relaxation times for LO-phonons are in agreement with the literature [48].

5. Conclusions

In this study, graphene layers were grown on 4H–SiC substrate with the Si sublimation method. After Hall bar fabrication, Hall effect measurements were carried out as a function of temperature (1.8–200 K) at a static magnetic field (0.5 T). Magnetic-field dependent Hall data were analyzed by using the SPCEM technique. By implementing SPCEM, bulk and 2D carrier densities and mobilities were extracted successfully. The bulk carrier is attributed to SiC substrate and the 2D carrier is attributed to the graphene layer. For the SPCEM extracted carrier data, proper 3D or 2D scattering analyses were performed.

The SPCEM extracted carrier data successfully explained the scattering analyses. The fit parameters and the overall results of both scattering analyses are in agreement with the literature. Temperature independent mobility components with the same mobility limiting value are observed for both scattering analyses. Because of this, these components may be related to the same interaction and/or related to a graphene–SiC layer interaction. Because the SPCEM gives results with some error at the investigated mid-temperatures [18], the low and high temperature results of the investigated temperature range are the most preferable. Therefore, with implementation of SPCEM, one can find extracted graphene mobility at high temperatures and effective ionized impurity density at low temperatures by using the temperature dependent static magnetic field Hall data.

Acknowledgments

This work is supported by the projects DPT-HAMIT, DPT-FOTON, NATO-SET-193 and TUBITAK under Project nos. 113F364, 113E331, 109A015, and 109E301. One of the authors (E.O.) also acknowledges partial support from the Turkish Academy of Sciences.

References

- [1] K.S. Novoselov, A.K. Geim, S.V. Morozov, D. Jiang, Y. Zhang, S.V. Dubonos, I.V. Grigorieva, A.A. Firsov, *Science* 306 (2004) 666.
- [2] D. Wei, Y. Liu, Y. Wang, H. Zhang, L. Huang, G. Yu, *Nano Lett.* 9 (2009) 1752.
- [3] C. Mattevi, G. Eda, S. Agnoli, S. Miller, K.A. Mkhoyan, O. Celik, D. Mastrogianni, G. Granozzi, E. Garfunkel, M. Chhowalla, *Adv. Funct. Mater.* 19 (2009) 2577.
- [4] I. Jung, D. Dikin, S. Park, W. Cai, S.L. Mielke, R.S. Ruoff, *J. Phys. Chem. C* 112 (2008) 20264.
- [5] Z. Chen, Y.-M. Lin, M.J. Rooks, P. Avouris, *Physica E* 40 (2007) 228.
- [6] S.Y. Zhou, G.-H. Gweon, A.V. Fedorov, P.N. First, W.A. de Heer, D.-H. Lee, F. Guinea, A.H. Castro Neto, A. Lanzara, *Nat. Mater.* 6 (2007) 770.
- [7] H. Hiura, M.V. Lee, A.V. Tyurnina, K. Tsukagoshi, *Carbon* 50 (2012) 5076.
- [8] P.W. Sutter, J.I. Flege, E.A. Sutter, *Nat. Mater.* 7 (2008) 406.
- [9] D. Li, M.B. Muller, S. Gilje, R.B. Kaner, G.G. Wallace, *Nat. Nanotechnol.* 3 (2008) 101.
- [10] C. Yu, J. Li, Q.B. Liu, S.B. Dun, Z.Z. He, X.W. Zhang, S.J. Cai, Z.H. Feng, *Appl. Phys. Lett.* 102 (2013) 013107.
- [11] M.J. Kane, N. Apsley, D.A. Anderson, L.L. Taylor, T. Kerr, *J. Phys. C: Solid State Phys.* 18 (1985) 5629.
- [12] S.P. Tobin, G.N. Pultz, E.E. Krueger, M. Kestigian, K.K. Wong, P.W. Norton, *J. Electron. Mater.* 22 (1993) 907.
- [13] W.A. Beck, J.R. Anderson, *J. Appl. Phys.* 62 (1987) 541.
- [14] J.R. Meyer, C.A. Hoffman, F.J. Arnold, S. Sivananthan, J.P. Faurie, *Semicond. Sci. Technol.* 8 (1993) 805.
- [15] Z. Dziuba, J. Antoszewski, J.M. Dell, L. Faraone, P. Kozodoy, S. Keller, B. Keller, S.P. DenBaars, U.K. Mishra, *J. Appl. Phys.* 82 (1997) 2996.
- [16] I. Vurgaftman, J.R. Meyer, C.A. Hoffman, D. Redfern, J. Antoszewski, L. Faraone, J.R. Lindemuth, *J. Appl. Phys.* 84 (1998) 4966.
- [17] J. Rothman, J. Meilhan, G. Perrais, J.-P. Belle, O. Gravrand, *J. Electron. Mater.* 35 (2006) 1174.
- [18] S.B. Lisesivdin, N. Balkan, E. Ozbay, *Microelectron. J.* 40 (2009) 413.
- [19] J.H. Davies, *The Physics of Low-Dimensional Semiconductors*, Cambridge University Press, Cambridge, 1998.
- [20] S.B. Lisesivdin, A. Yildiz, S. Acar, M. Kasap, S. Ozcelik, E. Ozbay, *Appl. Phys. Lett.* 91 (2007) 102113.
- [21] S. Gokden, *Phys. Status Solidi A* 200 (2003) 369.
- [22] N. Biyikli, J. Xie, Y.T. Moon, F. Yun, C.G. Stefanita, S. Bandyopadhyay, H. Morkoc, I. Vurgaftman, J.R. Meyer, *Appl. Phys. Lett.* 88 (2006) 142106.
- [23] J. Antoszewski, L. Faraone, *Opto-Electron. Rev.* 12 (2004) 347.
- [24] S.B. Lisesivdin, H. Altuntas, A. Yildiz, M. Kasap, E. Ozbay, S. Ozcelik, *Superlattices Microstruct.* 45 (2009) 604.
- [25] T.N. Theis, B.D. Parker, P.M. Solomon, S.L. Wright, *Appl. Phys. Lett.* 49 (1986) 1542.
- [26] R. Oberhuber, G. Zandler, P. Vogl, *Phys. Rev. B* 58 (1998) 9941.
- [27] B.K. Ridley, B.E. Foutz, L.F. Eastman, *Phys. Rev. B* 61 (2000) 16862.
- [28] D. Zanato, S. Gokden, N. Balkan, B.K. Ridley, W.J. Schaff, *Superlattices Microstruct.* 34 (2003) 77.
- [29] N.T. Son, W.M. Chen, O. Kordina, A.O. Konstantinov, B. Monemar, E. Janzen, D.M. Hofman, D. Volm, M. Drechsler, B.K. Meyer, *Appl. Phys. Lett.* 66 (1995) 1074.
- [30] L. Patrick, W.J. Choyke, *Phys. Rev. B* 2 (1970) 2255.
- [31] D. Sun, Z. Wu, C. Divin, X. Li, C. Berger, W.A. de Heer, P.N. First, T.B. Norris, *Phys. Rev. Lett.* 101 (2008) 157402.
- [32] S. Tanabe, Y. Sekine, H. Kageshima, M. Nagase, H. Hibino, *Phys. Rev. B* 84 (2011) 115458.
- [33] K. Kamitani, M. Grimsditch, J.C. Nipko, C.-K. Loong, M. Okada, I. Kimura, *J. Appl. Phys.* 82 (1997) 3152.
- [34] J.D. Wiley, in: R.K. Wilardson, A.C. Beer (Eds.), *Semiconductors and Semimetals*, vol. 10, Academic, New York, 1975.
- [35] B.L. Gelmont, M. Shur, M. Strosio, *J. Appl. Phys.* 77 (1995) 657.
- [36] J.H. Chen, C. Jang, S. Xiao, M. Ishigami, M. Fuhrer, *Nat. Nanotechnol.* 3 (2008) 206.
- [37] W. Zhu, V. Perebeinos, M. Freitag, P. Avouris, *Phys. Rev. B* 80 (2009) 235402.
- [38] S. Fratini, F. Guinea, *Phys. Rev. B* 77 (2008) 195415.
- [39] C.R. Dean, A.F. Young, I. Meric, C. Lee, L. Wang, S. Sorgenfrei, K. Watanabe, T. Taniguchi, P. Kim, K.L. Shepard, J. Hone, *Nat. Nanotechnol.* 5 (2010) 722.
- [40] D.K. Ferry, *Semiconductor Transport*, Taylor and Francis, London (2000) 122.
- [41] B.K. Ridley, *J. Phys. C: Solid State Phys.* 15 (1982) 5899.
- [42] M. Shur, B. Gelmont, M. Asif Khan, *J. Electron. Mater.* 25 (1996) 777.
- [43] J.R. Jenny, St.G. Müller, A. Powell, V.F. Tsvetkov, H.M. Hobgood, R.C. Glass, C.H. Carter Jr., *J. Electron. Mater.* 31 (2002) 366.
- [44] M. Ikeda, H. Matsunami, T. Tanaka, *Phys. Rev. B* 22 (1980) 2842.
- [45] J. Zhang, L. Storasta, J.P. Bergman, N.T. Son, E. Janzén, *J. Appl. Phys.* 93 (2003) 4708.
- [46] D.B. Farmer, V. Perebeinos, Y.M. Lin, C. Dimitrakopoulos, P. Avouris, *Phys. Rev. B* 84 (2011) 205417.
- [47] H. Nienhaus, T.U. Kampen, W. Monch, *Surf. Sci.* 324 (1995) L328.
- [48] H. Iwata, K.M. Itoh, G. Pensl, *J. Appl. Phys.* 88 (2000) 1956.